Correlations of ^{18}F-THK5351 PET with Postmortem Burden of Tau and Astrogliosis in Alzheimer Disease

Ryuichi Harada[1,2], Aiko Ishiki[2], Hideaki Kai[3], Naomi Sato[4], Katsutoshi Furukawa[2,5], Shozo Furumoto[6], Tetsuro Tago[7], Naoki Tomita[2], Shoichi Watanuki[6], Kotaro Hiraoka[6], Yoichi Ishikawa[6], Yoshihito Funaki[6], Tadaho Nakamura[8], Takeo Yoshikawa[1], Ren Iwata[6], Manabu Tashiro[6], Hironobu Sasano[4], Tetsuyuki Kitamoto[3], Kazuhiko Yanai[1,6], Hiroyuki Arai[2], Yukitsuka Kudo[2], and Nobuyuki Okamura[6,8]

[1]Department of Pharmacology, Tohoku University School of Medicine, Sendai, Japan; [2]Department of Gerontology and Geriatrics, Institute of Development, Aging and Cancer, Tohoku University, Sendai, Japan; [3]Department of Neurological Science, Tohoku University School of Medicine, Sendai, Japan; [4]Department of Pathology, Tohoku University School of Medicine, Sendai, Japan; [5]Division of Community Medicine, Faculty of Medicine, Tohoku Medical and Pharmaceutical University, Sendai, Japan; [6]Cyclotron and Radioisotope Center, Tohoku University, Sendai, Japan; [7]Research Team for Neuroimaging, Tokyo Metropolitan Institute of Gerontology, Tokyo, Japan; and [8]Division of Pharmacology, Faculty of Medicine, Tohoku Medical and Pharmaceutical University, Sendai, Japan

Clinical PET studies using ^{18}F-THK5351 have demonstrated significant tracer retention in sites susceptible to tau burden in Alzheimer disease (AD). However, the in vivo PET signal to reflect tau aggregates remains controversial. **Methods:** We examined the spatial pattern of tracer binding, amyloid-β, tau, and gliosis in an autopsy-confirmed AD patient who underwent ^{18}F-THK5351 and ^{11}C-Pittsburgh compound B PET before death. **Results:** Regional in vivo ^{18}F-THK5351 retention was significantly correlated with the density of tau aggregates in the neocortex and monoamine oxidase-B in the whole brain, but not correlated with that of insoluble amyloid-β. Furthermore, significant association was observed between the density of tau aggregates, monoamine oxidase-B, and glial fibrillary acidic protein, suggesting that neocortical tau would strongly influence the formation of reactive astrocytes. **Conclusion:** ^{18}F-THK5351 PET may have limited utility as a biomarker of tau pathology in AD; however, it could be used to monitor the neuroinflammatory processes in the living brain.

Key Words: Alzheimer's disease; tau; PET; imaging-pathology correlation

J Nucl Med 2018; 59:671–674
DOI: 10.2967/jnumed.117.197426

In vivo imaging of tau pathology would provide new insights into the pathogenesis of several neurodegenerative diseases, including Alzheimer disease (AD) (*1,2*). Recent efforts to develop tau-specific PET radiopharmaceuticals produced several promising candidates, including quinoline derivatives designed to detect tau aggregates (*1,3,4*). Clinical PET studies have demonstrated elevated tracer retention predominantly in the temporal cortex in patients with AD. Despite this evidence, the binding specificity of tau-targeting PET radiopharmaceuticals has yet to be determined. For example, ^{18}F-THK5351 demonstrates significant tracer binding in the basal ganglia, in which tau pathology is not prominent in AD (Fig. 1). Furthermore, a recent human blocking study demonstrated substantial reduction of ^{18}F-THK5351 retention after the administration of monoamine oxidase-B (MAO-B) inhibitor selegiline (*5*).

In this study, we examined the imaging data of the brain from an autopsy-confirmed AD patient who underwent ^{18}F-THK5351 and ^{11}C-Pittsburgh compound B (^{11}C-PiB) PET scans before death, to determine the correlation of antemortem in vivo THK5351 and PiB binding with quantitative measurements of neuropathologic substrates in the same brain regions of this patient.

MATERIALS AND METHODS

Participants

The study was approved by the Ethics Committee of the Tohoku University Graduate School of Medicine. Informed consent for neuroimaging and brain autopsy was obtained. The patient was an 81-y-old male with a 7-y history of progressive memory impairment and cognitive decline with delusion. He was clinically diagnosed with AD 3 y after the first symptoms appeared. ^{18}F-THK5351 and ^{11}C-PiB PET scans were performed 216 d and 600 d before death, respectively. At the time of the ^{18}F-THK-5351 PET scan, his Mini Mental State Examination and ADAS-cog (Alzheimer's Disease Assessment Scale-Cognitive Subscale) scores were 10 and 48.3, respectively. At autopsy, his brain weight was 1,230 g. Brain atrophy was observed in the amygdala; hippocampus; parahippocampal gyrus; and the frontal, temporal, and parietal cortices on gross examination. Atherosclerosis was also observed in the basilar artery, left internal carotid artery, and left middle cerebral artery. In this case, amyloid-β (Aβ) Thal phase was 5, Braak stage was VI, and the neuritic plaque score was frequent (A3, B3, C3) (*6*). Lewy pathology was also present in the amygdala and entorhinal cortex. However, TDP-43 inclusions were absent, although severe neuronal loss was observed in the hippocampus.

Image Acquisition

PET imaging was performed using an Eminence STARGATE PET scanner (Shimadzu). After intravenous injection of ^{18}F-THK5351 (185 MBq) or ^{11}C-PiB (296 MBq), dynamic PET images were obtained for 60 min (^{18}F-THK5351) or 70 min (^{11}C-PiB) with the patient's eyes

Received Jun. 12, 2017; revision accepted Jul. 25, 2017.
For correspondence or reprints contact: Ryuichi Harada, Department of Pharmacology, Tohoku University School of Medicine, 2-1, Seiryo-machi, Aoba-ku, Sendai, 9808575, Japan.
E-mail: dragon1@med.tohoku.ac.jp
Published online Sep. 1, 2017.

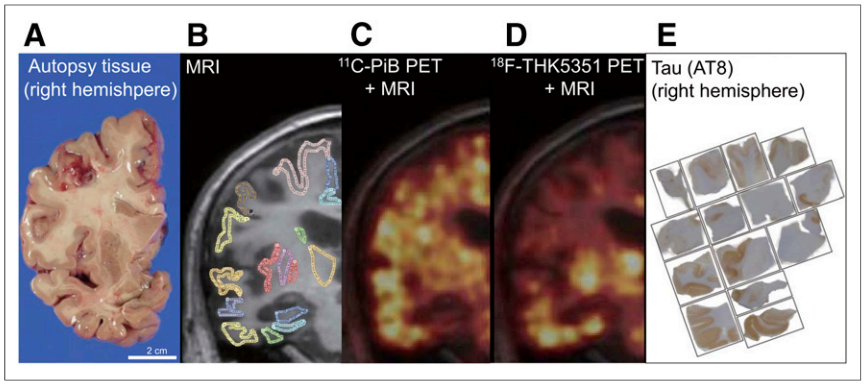

FIGURE 1. Images from coronal brain sections of autopsy tissue from right hemisphere (A), MRI with regions of interest (B), coregistered ^{11}C-PiB PET scan (C), coregistered ^{18}F-THK5351 PET scan (D), and tissue sections immunostained by anti-tau antibody (AT8) (E) in an AD patient (81-y-old man, Mini Mental State Examination Score 16 at PET scans).

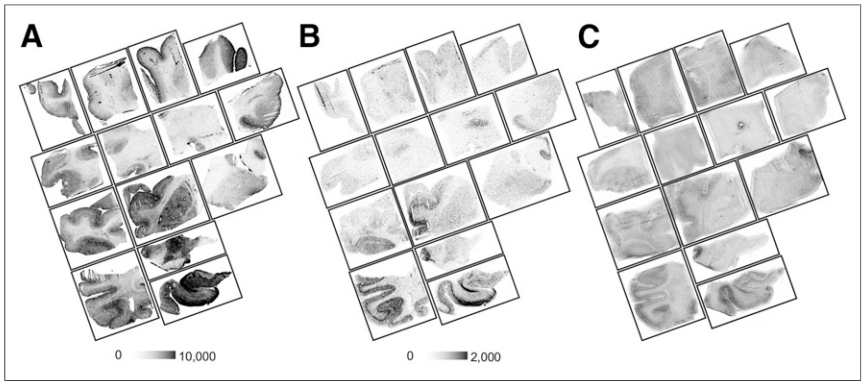

FIGURE 2. In vitro autoradiograms of ^{3}H-THK5351 in brain sections from a patient with AD (81-y-old man) in absence (A) and presence (B) of MAO-B inhibitor lazabemide. (C) Images of Gallyas-Braak silver staining.

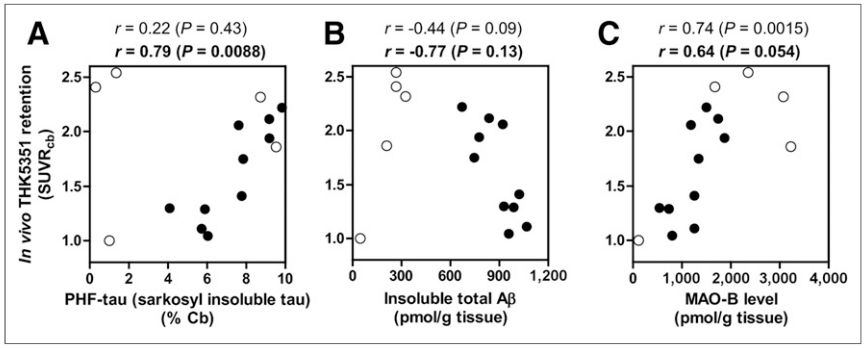

FIGURE 3. Correlation between antemortem in vivo ^{18}F-THK5351 PET SUVRs on PET scans with biochemical postmortem quantification of sarkosyl-insoluble tau (T46) (A), insoluble total Aβ (B), and MAO-B (C) in corresponding 15 regions from frozen right hemisphere. Correlation coefficients and *P* values in whole brain (regular) and neocortex (bold) are shown at the top of each graph. ● = neocortical area; ○ = other brain areas.

closed. T1-weighted MR images were obtained with a SIGNA 1.5-T machine (GE Healthcare) using a previously described method (*4*). SUV images of ^{18}F-THK5351 (40–60 min after injection) and ^{11}C-PiB (50–70 min after injection) were obtained by normalizing tissue radioactivity concentration by injected dose and body weight. The regional SUV–to–cerebellar cortex SUV ratio (SUVR) was used as an index of tracer retention. PET images were coregistered on MR images using SPM12 software (SPM12; Wellcome Department of Imaging Neuroscience, UCL). Regions of interest were drawn on the coregistered MR image using PMOD software (version 3.7; PMOD Technologies GmbH).

In Vivo–In Vitro Correlation Analyses

Neuropathologic diagnostic analysis was performed on sections from the fixed left hemisphere. Frozen tissue blocks were sampled from the approximately 2-cm-thick coronal tissue slab of the right hemisphere. Frozen tissues were sectioned from the 14 blocks using a cryostat for autoradiography and immunohistochemistry. In vitro autoradiography was performed using the same protocol as previously described except for frozen sections (*4*). Coregistered MR and PET images of the right hemisphere were oriented along the coronal plane. The corresponding regions of interest were drawn on the MR image (Fig. 1), and then transformed onto the coregistered ^{18}F-THK5351 and ^{11}C-PiB PET images. Frozen tissue samples from the corresponding regions were homogenized in phosphate-buffered saline and used for biochemical analyses and binding assays as previously described (*4*).

Statistical Analysis

Spearman rank correlation coefficients were calculated to examine the association between radiotracer binding, histopathology, and biochemical data. Statistical significance was defined at a P value of less than 0.05. This analysis was performed using GraphPad Prism software (GraphPad).

RESULTS

In autoradiography, ^{3}H-THK5351 binding was substantially reduced in the presence of MAO-B inhibitor lazabemide, whereas ^{3}H-THK5351 binding in AD brains remained detectable and was consistent with the distribution of tau deposits (Fig. 2). There was a strong correlation between in vivo THK5351 binding and tau immunohistochemistry in the neocortex ($r = 0.96$, $P < 0.0001$) (Supplemental Fig. 1; supplemental materials are available at http://jnm.snmjournals.org). A similar correlation was also found between in vivo THK5351 binding and argyrophilic neurofibrillary pathology detected by Gallyas–Braak staining ($r = 0.89$, $P < 0.0001$). However, the significance of these correlations was diminished when subcortical regions were included in this analysis. A significant correlation was additionally observed between in vivo THK5351 retention and in vitro ^{3}H-THK5351 binding in postmortem brain sections ($r = 0.54$,

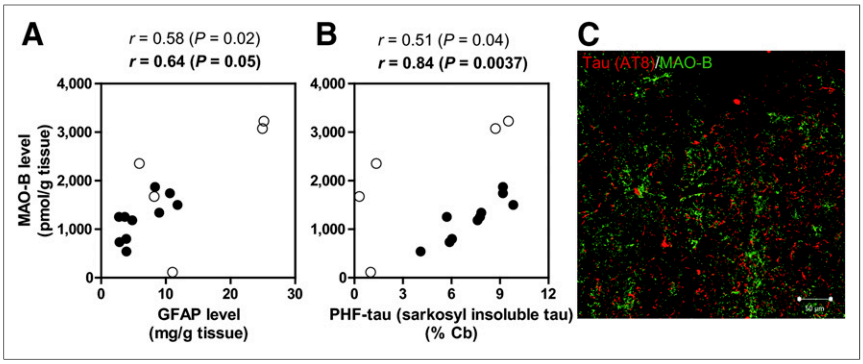

FIGURE 4. Correlation of MAO-B with GFAP (A) and PHF-tau (B) levels. Immunofluorescence double staining image of AT8 and MAO-B. (C) Correlation coefficients and *P* values in whole brain (regular) and neocortex (bold) are shown at the top of each graph. ● = neocortical area; ○ = other brain areas.

$P = 0.03$). There was no correlation between in vivo THK5351 binding and Aβ plaque load. Biochemical analyses were compatible with those determined by immunohistochemistry. In vivo THK5351 retention in the neocortex was strongly correlated with insoluble paired helical filaments (PHF)-tau level ($r = 0.79$, $P = 0.0088$), but not with insoluble Aβ level (Fig. 3). The regional MAO-B level was significantly correlated with in vivo THK5351 retention in the whole brain ($r = 0.74$, $P = 0.0015$). In contrast, in vivo PiB binding was significantly correlated with insoluble Aβ ($r = 0.55$, $P = 0.03$), but not with PHF-tau and MAO-B levels (Supplemental Fig. 2).

As demonstrated in previous studies, MAO-B is abundant in astrocytes. In fact, regional MAO-B levels were positively correlated with glial fibrillary acidic protein (GFAP) levels in this patient (Fig. 4A). The spatial distribution of PHF-tau in the neocortex of this AD patient was very similar to that of MAO-B (Fig. 4B). Double staining showed no colocalization between tau and MAO-B (Fig. 4C), indicating that these 2 proteins were separately located in neurons and astrocytes.

DISCUSSION

Clinical PET studies using putative tau-specific tracers have demonstrated significant tracer retention in sites susceptible to tau burden in AD patients (*1,2*). However, recent studies have also suggested the potential contribution of off-target tracer binding to PET images. In the present study, we examined correlations between in vivo tracer binding and neuropathologic substrates in postmortem brain tissues from an AD patient who underwent ^{18}F-THK5351 and ^{11}C-PiB PET before death.

In our imaging-pathology correlation analysis, in vivo cortical ^{18}F-THK5351 retention correlated with PHF-tau and MAO-B, but not with Aβ, in postmortem AD brains. In the autoradiography of AD brain sections, the specific binding of ^{3}H-THK5351 in the neocortex remained even in the presence of MAO-B inhibitors, and correlated with the density of PHF-tau. Thus, it can be said that THK5351 binding to PHF-tau contributes to in vivo PET signals in patients with AD. However, we also observed that ^{3}H-THK5351 binding was substantially blocked in the presence of a MAO-B inhibitor. This was consistent with recent results from a human blocking study showing that a substantial reduction of ^{18}F-THK5351 retention was observed after the administration of the MAO-B inhibitor selegiline (*5*). Our data demonstrated that in vivo ^{18}F-THK5351 retention in the neocortex correlated not only with PHF-tau, but also with MAO-B levels in the brain. Collectively, these data suggest that THK5351 binding to MAO-B greatly contributes to in vivo PET signals. Further studies are required to clarify what percentage of the ^{18}F-THK5351 PET signal was derived from MAO-B and PHF-tau.

MAO-B is predominantly expressed in the outer membrane of astrocyte mitochondria, which are widely distributed in human brains. MAO-B levels increase linearly in an age-dependent manner in whole-brain regions during the normal aging processes (*7,8*). A significant correlation has been observed between GFAP immunoreactivity and MAO-B inhibitor binding in AD brain (*9*). The present study also demonstrated the significant correlation between MAO-B and GFAP levels in AD brains, indicating that the level of THK5351 binding is likely associated with astrogliosis. Postmortem binding studies with ^{3}H-L-deprenyl and ^{3}H-lazabemide have shown the elevation of MAO-B levels in AD brains (*9–11*). Furthermore, in vivo PET studies using ^{11}C-L-deprenyl have demonstrated elevated tracer uptake in the brains of AD patients (*12,13*). A large cross-sectional postmortem study has suggested that astrogliosis increased linearly throughout the disease course and correlated with tau pathology and brain atrophy, but not with amyloid plaques (*14*). Neuroinflammatory elements such as reactive astrocytes and activated microglia are considered to be secondary processes after Aβ accumulation, although they progress together with tau pathology and contribute to neurodegeneration throughout the course of AD (*15*). ^{18}F-THK5351 PET can thus be used to track the progression of AD, by detecting both tau and reactive astrocytes.

CONCLUSION

^{18}F-THK5351 PET signal reflects the combination of tau pathology and reactive astrocytes. These findings suggest ^{18}F-THK5351 PET has limited utility for selective detection of tau pathology. However, this tracer has potential utility for the assessment of tau-associated neuroinflammatory changes in AD.

DISCLOSURE

This study was supported by research funds from GE Healthcare; the SEI (Sumitomo Electric Industries, Ltd.) Group CSR Foundation; Health and Labor Sciences Research Grants from the Ministry of Health, Labor, and Welfare of Japan; Grant-in-Aid for Scientific Research (B) (15H04900); Grant-in-Aid for Young Scientists (B) (15K19767); Grant-in-Aid for Scientific Research (B) (25293259); Grant-in-Aid for Scientific Research on Innovative Areas (Brain Protein Aging and Dementia Control) (26117003) from MEXT; and the Japan Research Foundation for Clinical Pharmacology. No other potential conflict of interest relevant to this article was reported.

REFERENCES

1. Okamura N, Harada R, Furumoto S, Arai H, Yanai K, Kudo Y. Tau PET imaging in Alzheimer's disease. *Curr Neurol Neurosci Rep*. 2014;14:500.
2. Villemagne VL, Fodero-Tavoletti MT, Masters CL, Rowe CC. Tau imaging: early progress and future directions. *Lancet Neurol*. 2015;14:114–124.

3. Villemagne VL, Dore V, Bourgeat P, et al. Aβ-amyloid and tau imaging in dementia. *Semin Nucl Med*. 2017;47:75–88.
4. Harada R, Okamura N, Furumoto S, et al. ^{18}F-THK5351: a novel PET radiotracer for imaging neurofibrillary pathology in Alzheimer disease. *J Nucl Med.* 2016;57: 208–214.
5. Ng KP, Pascoal TA, Mathotaarachchi S, et al. Monoamine oxidase B inhibitor, selegiline, reduces ^{18}F-THK5351 uptake in the human brain. *Alzheimers Res Ther.* 2017;9:25.
6. Hyman BT, Phelps CH, Beach TG, et al. National Institute on Aging-Alzheimer's Association guidelines for the neuropathologic assessment of Alzheimer's disease. *Alzheimers Dement.* 2012;8:1–13.
7. Fowler JS, Volkow ND, Wang GJ, et al. Age-related increases in brain monoamine oxidase B in living healthy human subjects. *Neurobiol Aging*. 1997;18:431–435.
8. Tong J, Meyer JH, Furukawa Y, et al. Distribution of monoamine oxidase proteins in human brain: implications for brain imaging studies. *J Cereb Blood Flow Metab*. 2013;33:863–871.
9. Saura J, Luque JM, Cesura AM, et al. Increased monoamine oxidase B activity in plaque-associated astrocytes of Alzheimer brains revealed by quantitative enzyme radioautography. *Neuroscience*. 1994;62:15–30.
10. Gulyás B, Pavlova E, Kasa P, et al. Activated MAO-B in the brain of Alzheimer patients, demonstrated by [^{11}C]-L-deprenyl using whole hemisphere autoradiography. *Neurochem Int.* 2011;58:60–68.
11. Marutle A, Gillberg PG, Bergfors A, et al. ^{3}H-deprenyl and ^{3}H-PIB autoradiography show different laminar distributions of astroglia and fibrillar beta-amyloid in Alzheimer brain. *J Neuroinflammation*. 2013;10: 90.
12. Santillo AF, Gambini JP, Lannfelt L, et al. In vivo imaging of astrocytosis in Alzheimer's disease: an ^{11}C-L-deuteriodeprenyl and PIB PET study. *Eur J Nucl Med Mol Imaging*. 2011;38:2202–2208.
13. Carter SF, Scholl M, Almkvist O, et al. Evidence for astrocytosis in prodromal Alzheimer disease provided by ^{11}C-deuterium-L-deprenyl: a multitracer PET paradigm combining ^{11}C-Pittsburgh compound B and ^{18}F-FDG. *J Nucl Med*. 2012;53:37–46.
14. Serrano-Pozo A, Mielke ML, Gomez-Isla T, et al. Reactive glia not only associates with plaques but also parallels tangles in Alzheimer's disease. *Am J Pathol.* 2011;179:1373–1384.
15. Ingelsson M, Fukumoto H, Newell KL, et al. Early Aβ accumulation and progressive synaptic loss, gliosis, and tangle formation in AD brain. *Neurology.* 2004;62:925–931.